View metadata, citation and similar papers at core.ac.uk

brought to you by CORE

provided by Scholarworks@GVSU

Grand Valley State University
ScholarWorks@GVSU

Honors Projects | Undergraduate Research and Creative Practice

5-2016

Spurious Acceleration Noise on the LISA Spacecraft Due to Solar Irradiance

Brandon Piotrzkowski
Grand Valley State University

Follow this and additional works at: http://scholarworks.gvsu.edu/honorsprojects


Part of the Physical Sciences and Mathematics Commons

Recommended Citation
Piotrzkowski, Brandon, "Spurious Acceleration Noise on the LISA Spacecraft Due to Solar Irradiance" (2016). *Honors Projects*. 581.
http://scholarworks.gvsu.edu/honorsprojects/581

This Open Access is brought to you for free and open access by the Undergraduate Research and Creative Practice at ScholarWorks@GVSU. It has been accepted for inclusion in Honors Projects by an authorized administrator of ScholarWorks@GVSU. For more information, please contact scholarworks@gvsu.edu.

Spurious Acceleration Noise on the LISA Spacecraft Due to Solar Irradiance

Brandon Piotrzkowski[1,*]

[1]*Department of Physics, Grand Valley State University, Allendale, MI 49504*

Abstract

The Laser Interferometer Space Antenna (LISA) is a configuration of three satellites that will very precisely measure the distance between each satellite in order to detect gravitational waves, small undulations in spacetime.[1] Therefore, the stability of LISA satellite configuration will be crucial to its ability to measure gravitational waves, as will understanding the noise introduced in the measured gravitational wave signal from various environmental accelerations. Although solar irradiance will most definitely be a great source of noise in the desired frequency band and will greatly attempt to disrupt the satellite configuration, previous research has only considered zeroth order calculations of force on the satellites by irradiance in static systems. To remedy this, we used a geometric and material based approach to calculate the force on the satellites solar arrays, the only component facing the sun. Running our simulation of LISA based on irradiance data from the VIRGO (Variability of solar IRadiance and Gravity Oscillations) experiment, we examined the Fourier transform of force to find the associated acceleration noise expected in the LISA frequency band due to solar irradiance.[2] This research will help engineers in the construction of the solar array as well as help isolate the gravitational wave signal when LISA is flown.

*Electronic address: piotrzkb@mail.gvsu.edu

I. INTRODUCTION

Gravitational waves are essentially small undulations in spacetime, manifesting themselves by increasing and decreasing the distance between objects in a periodic fashion (see figure 1.) Gravitational waves are created whenever the third time derivative of the quadrople moment of the stress-energy tensor of a system is non-zero. In other words, if the system is accelrating without spherical symmetry it will emit gravitational waves.[3] Common astrophysical examples of this are binary systems, spinning non-spherical objects, and supernovae. Mathematically, the form of gravitational waves can be shown by linearizing the metric equation so that the metric is flat ($\eta_{\mu\nu}$) with a very small pertubation ($h_{\mu\nu}$) such that

$$g_{\mu\nu} = \eta_{\mu\nu} + h_{\mu\nu}$$

where $|h_{\mu\nu}| \ll 1$. This assumption is valid if we are far from the source creating the gravitational waves. Since the focus of this paper is on noise characterization on a gravitational wave detector and not on gravitationals themselves, we will give only a brief overview of this derivation. Using this metric in the Einstein equation and invoking various guage conditions while assuming we are in a vacuum, the Einstein equation becomes

$$\Box^2 H^{\mu\nu} = 0$$

where $H^{\mu\nu}$ is the trace-reversed metric perturbation. This has solutions of

$$H^{\mu\nu}(t, x, y, z) = A^{\mu\nu} \cos(\vec{k} \cdot \vec{r} - \omega t)$$

where $\vec{k}$ is a wave-number vector, ω is the frequency, and $A^{\mu\nu}$ is a contant matrix.[3] $A^{\mu\nu}$ can be shown to have only two polarizations by invoking the transverse-traceless guage and forcing the wave to move down an axis (z-axis in this example) such that

$$A^{\mu\nu} = A_+ \begin{bmatrix} 0 & 0 & 0 & 0 \\ 0 & 1 & 0 & 0 \\ 0 & 0 & -1 & 0 \\ 0 & 0 & 0 & 0 \end{bmatrix} + A_\times \begin{bmatrix} 0 & 0 & 0 & 0 \\ 0 & 0 & 1 & 0 \\ 0 & 1 & 0 & 0 \\ 0 & 0 & 0 & 0 \end{bmatrix}$$

where A_+ and $A_\times$ are the amplitudes of each respective polarization. A visualization of these polarizations can be found in figure 1.

Although a necessary consequence of general relativity, they have only recently been directly measured by the LIGO (Laser Interferometer Gravitational-Wave Observatory) detector. The GW150914 detecton not only showed that gravitational waves are diretely measurable but we can obtain additional astrophysical information that optical telescopes alone cannot give, such as mass and separation distance in binary systems.[4] Gravitational wave detection is currently a huge focus for today's general relativists, as existing detectors such as LIGO and builders of future proposed detectors such as LISA (Laser Interferometer Space Attenna) now want use gravitational waves detection as an astrophysical tool to probe the cosmos. However, different projects like LISA and LIGO will not be sensitive to the same frequency spectrum, and therefore will not measure the same astrophysical sources. Since LISA will be focusing on the lower frequencies ($10^{-4} - 1$ Hz), its targeted sources

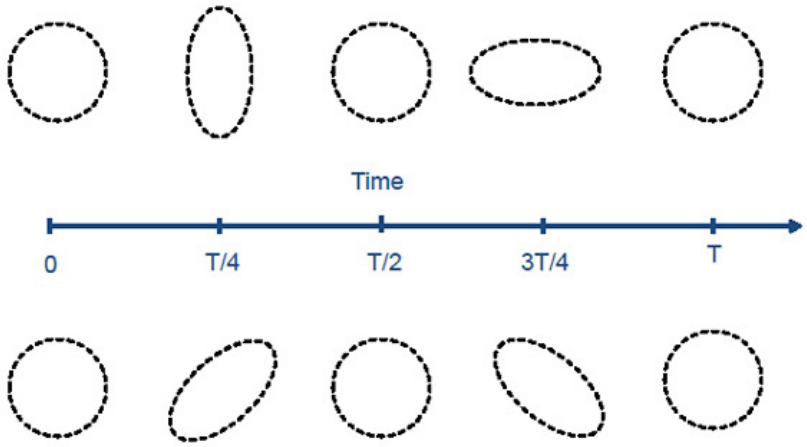

FIG. 1: Visual of the effect of both polarizations of a passing gravitational wave on test masses in space. Credit: *Scientific American*.

will be the merger of massive black hole binaries with masses 10^2 to 10^7 $M_\odot$ (solar mass), compact stellar objects spiralling into large black holes (with masses $\geq 10^5$ $M_\odot$), and close compact stellar binaries.[5] Meanwhile LIGO, looking at frequencies ($1 - 1000$ Hz), will look at neutron star (≈ 1.4 $M_\odot$) and black hole binaries (near 10 $M_\odot$) during their inspiral, spinning neutron stars, and Type-II supernovae.[6] Figure 2 shows the many gravitatational wave sources and which detectors will be able to see them. Therefore both experiments will be necessary to see more of the spectrum that gravitational waves offers. However, both of these experiments are incredibly delicate and require measuring the changes of distance in range of $10^{-15} - 10^{-12}$ m. This means that isolating gravitational wave signal from noise introduced by its surrounding enviroment, a tactic that will give more precision and consequently give greater resolution of sources to the signal, is of great importance for when these signals are available and applied for research.

Solar irradiance will be the largest source of enviromental noise on LISA by a large margin and will consequently disrupt the relative orbits of the three spacecraft that comprise LISA, making onboard ion thrusters a necessity. Therefore we are motived to answer the following questions: *What effect does solar irradiance have scross the LISA frequency band and what is its characterization/frequency dependence? Is the force ever great enough during solar maximum or minimum so that LISA must be flown at certain periods of the solar cycle?*

In this paper we will discuss properties of an individual LISA spacecraft, how the three satellites measure gravitational waves, and the relevant instrumentation (solar array). We will discuss briefly how we calculate force by irradiance on a LISA satellite starting from general radiation pressure and then incorporating geometry as well as blackbody constants of the materials. Next we will discuss the dataset we used and how we handled the data and the fourier transform. Lastly we will discuss the results of the study.

II. CHARACTERISTICS OF THE LISA SPACECRAFT

Each LISA spacecraft orbits in its own Keplerian orbit, forming a triangular formation (constellation) around the sun about 20° behind the earth with approximate distance of

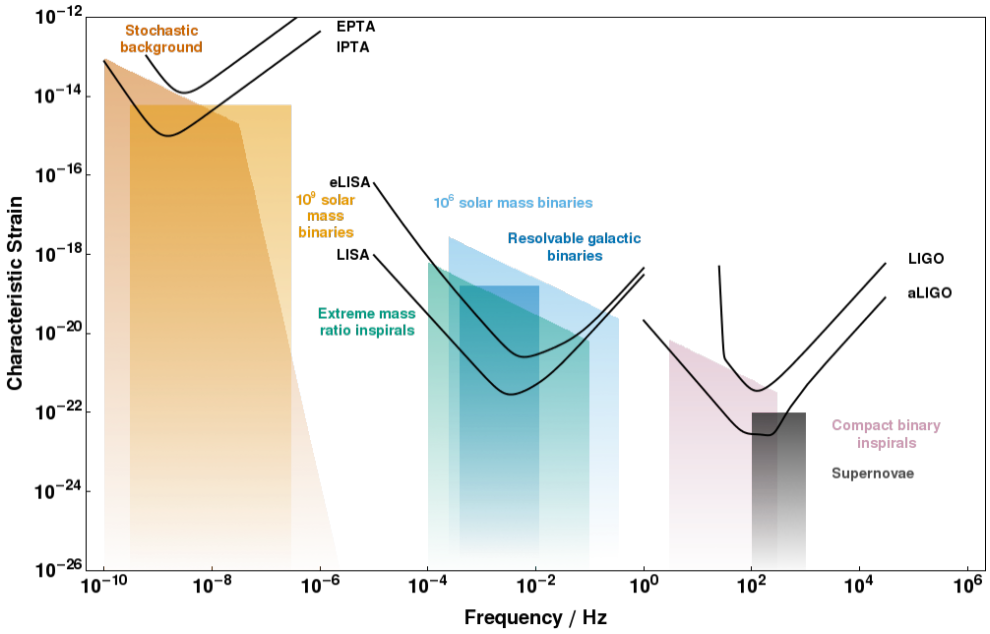

FIG. 2: Characteris strains and frequecies of various astrophysical sources and detectors. Credit: *University of Cambridge.*

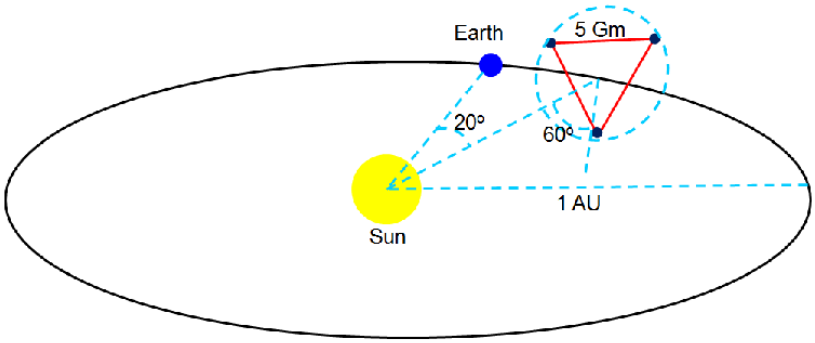

FIG. 3: Diagram of LISA position and formation. Credit: *NASA.*

5 million km between each craft. LISA will detect gravitational waves by calculating the distance between each spacecraft, done essentially by measuring the intensity of laser signals sent from a one craft to another. When a signal is received the spacecraft references the position of a test mass, free floating and located inside, and measures the phase difference between the signal is sending out and the one it received. Combining this information from the three arms comprises the gravitational wave signal. This process can only function if the test mass inside each spacecraft is free floating. Essentially the outer sections of the satellite are created to protect and house the test mass in order to prevent any external enviromental accelerations. Each spacecraft can compensate for constant accelerations by firing thrusters to keep itself centered on the test mass but even changing the center of mass will cause the test mass to accelerate, creating noise in the signal. Therefore it is crucial to understand all external force in general, although we will focus on irradiance since it will be the largest force and whether this force by irradiance will have any periodicities within the

LISA frequency band.

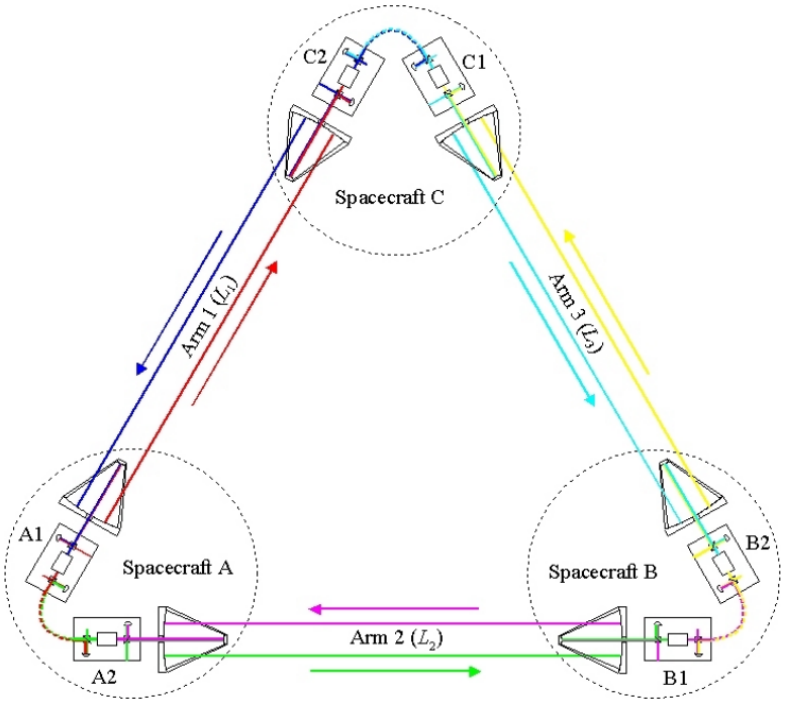

FIG. 4: Diagram of LISA position and formation. Credit: *NASA*.

Each spacecraft basically consists of a flat solar panel and a housing which contains the instruments (see Figure 5).[5] The solar panels not only function to provide power but also shield the instrument from the harmful solar winds and particles, as well as reduce thermal gradients across the equipment. This means that all force calculations of irradiance on the spacecraft will simply be the force on the solar array. Since each spacecraft turns while orbiting so that the solar array normal is about 30° above the solar plane, our calculations of force by irradiation will be fairly geometrically simple.

We will then primarily concern ourselves with the force on the solar array, both the direct force by radiation and the force by re-reradiation of the solar panel. To note, there are two different materials that make up the solar array: solar cells and optical solar reflectors (see Figure 5). The solar cells are used to generate electrical power for the rest of the components, and since several layers of cells are used in modern designs, we should be able to treat the solar cells as blackbodies since they absorb light efficiently across the frequency spectrum emitted by the sun. The optical solar reflectors are meant to relflect light for the purpose of reducing the overall temperature, placed wherever solar cells would not fit. Since each of these materials will have difference optical properties (absorbitivity, emissivity), we must consider the properties of both materials when performing force calculations. Lastly, we should note that solar arrays are typically manufactured with a coverglass that rejects frequencies of light that lie outside of the effective range of the solar cells (wavelengths from smaller than 300 nm and larger than 1350 nm.) We compensate for this effect by using Planck's Law (this is discussed in the Appendix). In addition, we can assume that the solar array is being manufactured so that is is thermally isolated from the rest of the components. Otherwise, the solar array would create temperature gradients within the equipment that

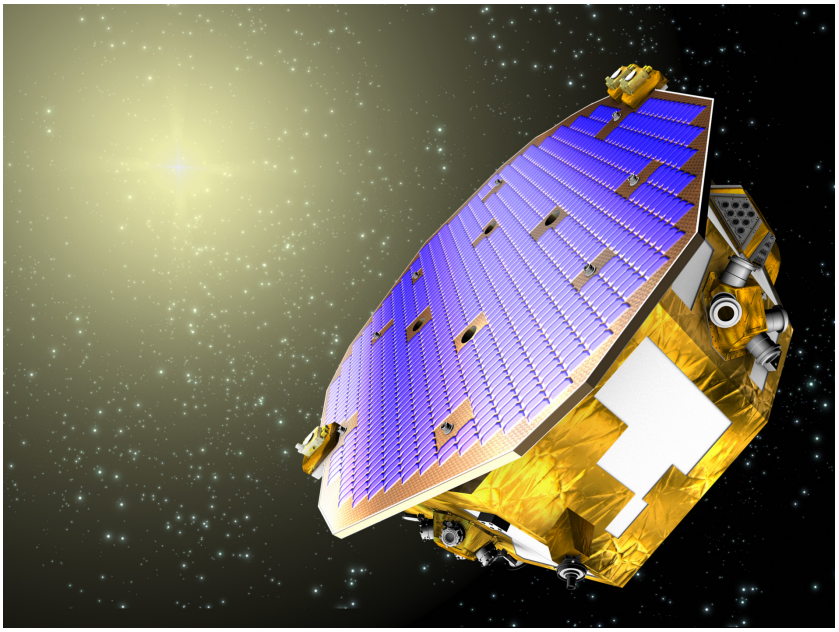

FIG. 5: Artist's rendition of LISA Pathfinder. Credit: *NASA*.

would certainly affect the test mass. So we need only consider the top side when calculating the force by re-radiation.

III. FORCE CALCULATIONS

We will derive the force in two parts, first force by direct solar irradiation and then force by reradiation. Although the details are shown in the Appendix, to calculate force we can expand from a simple case to one more general that pertains to our particular scenario. Note that will be using GSE (Geocentric Solar Ecliptic) coordinates visualized in Figure 3.

A. Force by Solar Irradiance

A zeroth order calculation of force by solar irradiance is given as

$$\vec{F_I} = -\frac{E_f A}{c}\hat{x} \tag{3.1}$$

where E_f is the solar energy flux or irradiance at 1 AU (W/m^2), A is area ($A = \pi r^2 \cos a$, where a is the angle between the normal and sun), and c is the speed of light.[7] Here we have a negative sign because we are using GSE coordinates; the x-axis points towards the sun. Expanding this for a rotated surface, remembering the that normal vector of LISA will be 30° from the plane of the solar system, with two materials gives us

$$\vec{F_I} = \begin{bmatrix} F_{I,x} \\ F_{I,z} \end{bmatrix} = -\frac{E_f}{c}\left(A_{sc} \begin{bmatrix} 1 + (1-\delta\alpha_{sc})\cos 2a \\ (1-\delta\alpha_{sc})\sin 2a \end{bmatrix} + A_{osr} \begin{bmatrix} 1 + (1-\delta\alpha_{osr})\cos 2a \\ (1-\delta\alpha_{osr})\sin 2a \end{bmatrix} \right) . \tag{3.2}$$

Here α_{sc} and α_{osr} are the absorbances of the solar cells and the optical solar reflectors respectively, A_{sc} and A_{osr} are the areas of the solar cells and the optical solar reflectors, and

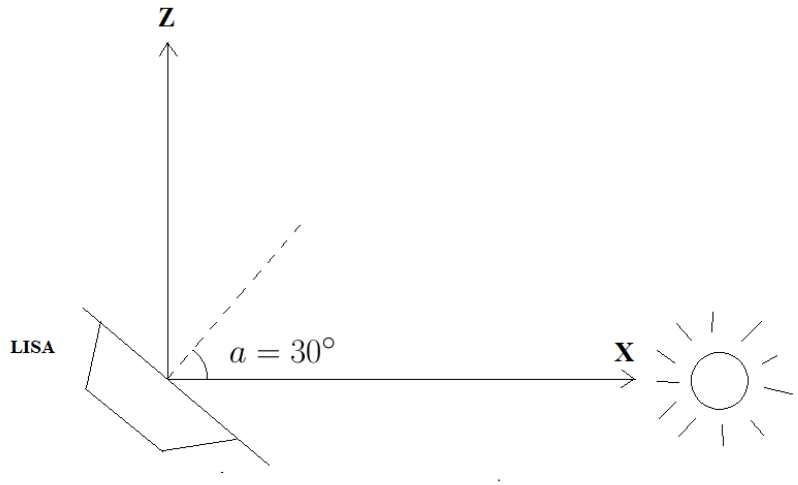

FIG. 6: A visual rendition of GSE coordinates. Here $\vec{x}$ points towards the sun, $\vec{z}$ points towards the ecliptic north pole, and $\vec{y} = \vec{z} \times \vec{x}$.

δ is the fractional power from irradiance delivered to the solar array, through the coverglass. Note that $2a$ is used instead of a since by rotating 45° all reflected irradiance should go entirely in the z-direction.

B. Force by Re-radiation

Again, note that this discussion is an abbreviation. Full details can be found in the Appendix A. We can first find the steady-state temperature of the solar array by finding when the power absorbed and reemitted are equal

$$(\alpha_{sc}A_{sc} + \alpha_{osr}A_{osr})\,\delta E_F = (\epsilon_{sc}A_{sc} + \epsilon_{osr}A_{osr})\,\sigma T_{sat}^4$$

where ϵ_{sc} and ϵ_{osr} are the emissivities of the solar cells and optical solar reflectors and σ is the Stephan-Boltzman constant. Solving for T and letting $A_r = A_{osr}/(A_{osr} + A_{sc})$ we have

$$T_{sat} = \left(\delta \frac{\alpha_{sc}(1 - A_r) + \alpha_{osr}A_r}{\epsilon_{sc}(1 - A_r) + \epsilon_{osr}A_r} \frac{E_f}{\sigma}\right)^{1/4} . \tag{3.3}$$

Solving for (3.1) by letting $E_f = \epsilon\sigma T^4$ and applying our specific conditions again, we have

$$\begin{bmatrix} F_x \\ F_z \end{bmatrix} = -\frac{1}{\pi}\left(\epsilon_{sc}(1 - A_r) + \epsilon_{osr}A_r\right) \frac{\sigma T_{sat}^4}{c} \begin{bmatrix} \cos a \\ \sin a \end{bmatrix} . \tag{3.4}$$

We can calculate force using (3.2) and (3.4) but this will inevitably be a time-dependent quantity. Of course, we aren't interested in the general force but simply forces with frequecies within the LISA sensitivity range ($10^{-4} - 1$ Hz). This means that we must examine a Fourier transform of force.

IV. DATA

We used the 60 second averaged total solar irradiance data, from 1996-2014, measured by the VIRGO (Variability of solar IRradiance and Gravity Oscillations) experiment aboard the SOHO (Solar and Heliospheric Observatory) spacecraft, which measures solar irradiance at the L1 (first Lagrangian) point. The 1/60 Hz sampling rate was chosen to allow us to see as much of the LISA frequency spectrum as possible (recall that LISA's frequency spectrum is$10^{-4} - 1$ Hz while the Nyquist frequency of this sampling rate is $1/120 \approx .0833$ Hz,allowing us to see any frequencies smaller than the Nyquist frequency). This data is normally used for helioseismology, which requires detection of high frequency phenomena, similar to our needs. The 60 second data points give us enough resolution to detect noise in the majority of the LISA frequency band. Using equations (3.2) and (3.4), along with absorbance/emissivity constants from modern solar array manufacturers, we calculated force on a LISA satellite over one and a half solar cycles (FIG. 4).[8]

V. METHODS OF FOURIER TRANSFORMATION

A. Basics of a Fourier Transform

To perform the Fourier transform we used the internal fast fourier transform (fft) command within NumPy, a common Python package. Mathematically this means we creating a frequency-dependent form of our force function, which is dependent on time, given by

$$\mathcal{F}\left[F(f_m)\right] = \sum_{n=0}^{N-1} F(t) e^{-2\pi i f_m t_n} \tag{5.1}$$

where f_m is a frequency (where m is an integer $0 \leq m \leq N-1$), N is the total number of points, t_n is a time, and $F(t)$ is the time function (force(t) in our case).[9] This sum will only give us the fourier transform of the particular frequency f_m, so this operation must be formed for all m, giving us a total number of N^2 calculations (note that modern algorithms only requre $N \log_2(N)$ so the model proposed here is simplified). We then plot $\mathcal{F}\left[F(f)\right]$ vs f to get our fourier transform. We also windowed our data with the tukey window, a mix between a hanning and rectange window, with an $\alpha = .5$ (the α values indicates whether the window is more like a rectangular window ($\alpha = 0$) or a hanning window ($\alpha = 1$)) (see Figure 7). Windowing used to accomodate the fact that discrete Fourier transforms occur over a finite region and to minimize the dropoff at each end.

Our first contention with the data is that the 60 second sampling rate will inevitably limit the frequencies. Nyquist theorem states that the highest frequency we can see in the Fourier transform is

$$f_N = \frac{1}{2 \cdot 60} = .08333 Hz \tag{5.2}$$

Unfortunately we will not be able to discuss any noise introduced by solar irradiance in the range $.083 - 1$ Hz.

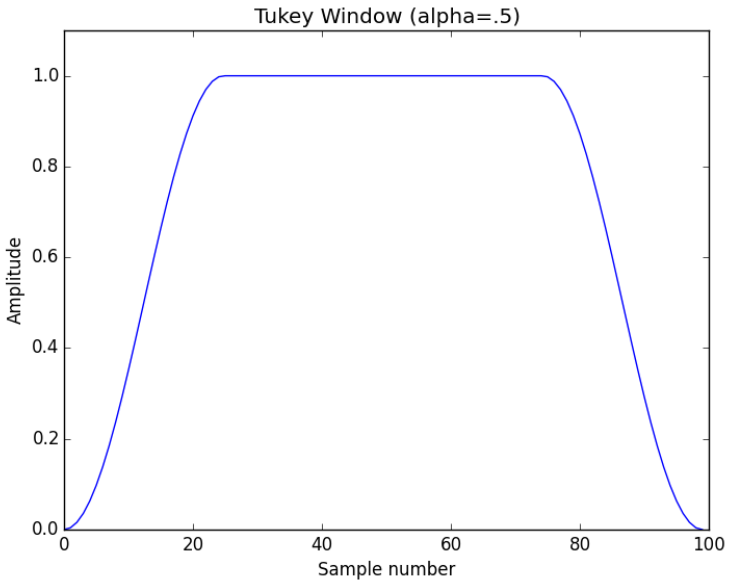

FIG. 7: Visual representation of the tukey window with $\alpha = .5$

B. The Gap Situation and Filling Methods

The major problem with our data is the fact is that there is many missing data points, or 'gaps', that must be dealt with since a fourier transform requires a complete data set. These gaps come from periods where the instruments were not taking data, due to failure, or the data was considered to be unreliable by the VIRGO research team. To examine the extent of data lost, we plotted the number of occurrences vs gap length as well as number of occurrences vs data length. These graphs are located in Appendix B.

There are a few conclusions that we can draw: the vast majority of gaps are very small and most of our data is continuous (around 300-700 data points in length before hitting a gap, refer to figures 14 through 17). This means that we only need to focus local filling techniques, since more gaps are small and large gaps are few in number, so filling them should have a neglible effect on the final fourier transform. In general, since most of the data is intact, our data should be fairly resistant to filling methods.

After and exhaustive study, we chose to use the averaging filling method. This means that we took the first value from either side of the gap and set every value in the gap to the average. Visually this looks like figure 8.

The reason we used this technique as opposed to something more complicated is because we found no real benefit to doing so. Take for example a linear filling technique, where you draw a line from one value to another as shown in figure 8.

We compared both techniques against a dataset that had no gaps, so we know what the ideal fourier transform looks like, we took out gaps, and then filled the gaps two ways, one with averaging and one with linear filling, and we took a fourier transfrom of each respective filled dataset. This result is shown in figure 9. Also we also tried the same comparrison method using the VIRGO dataset

As shown in figure 9 and 10, there is not a significant enough difference between the techniques to warrant switching to the the linear technique. Since switching to linear filling

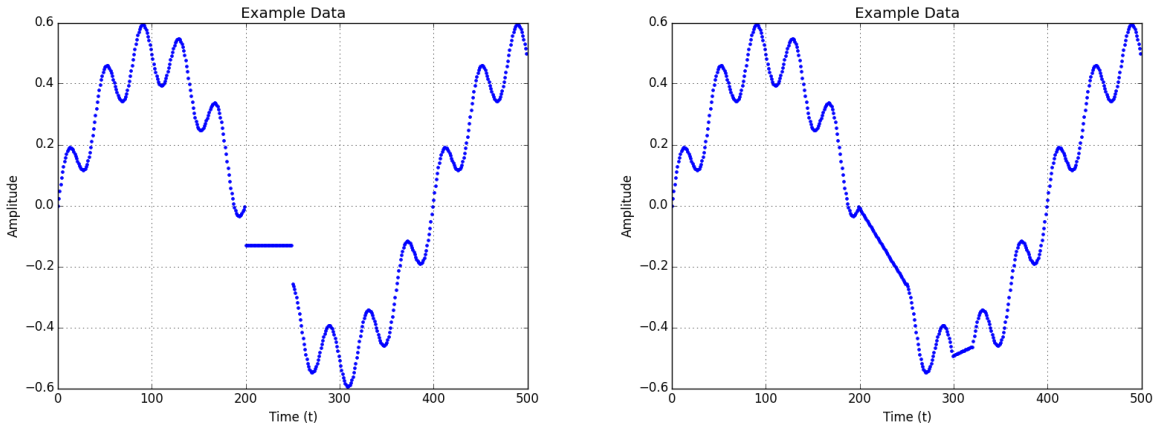

FIG. 8: Visual demonstration of the averaging and linear gap filling techniques.

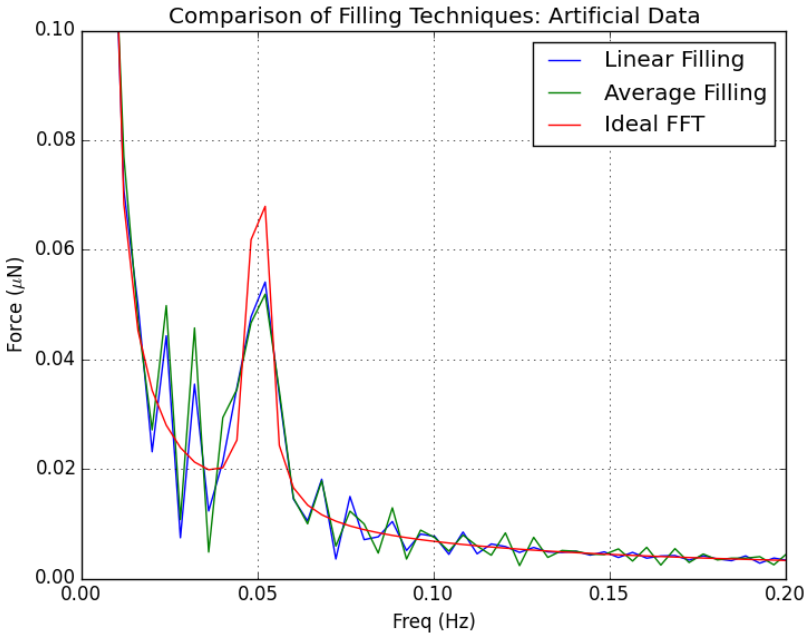

FIG. 9: Visual comparison of both averaging and linear gap filling techniques.

should've been the largest correction to averaging, any higher order interpolations should even have less correction so they can be neglected.

VI. RESULTS

Inspection of the force vs time graph (figure 11) reveals that the force stays within a narrow range and is nowhere near the $150\mu N$ limit of the combined four thrusters, a limit given to us after a conversation with NASA scientists Curt Cuttler and Guido Miller.[1] Of interest would be the combination of irradiance, solar wind, and perhaps acceleration from a passing asteroid, but otherwise irradiance will not push a satellite out of orbit by itself.

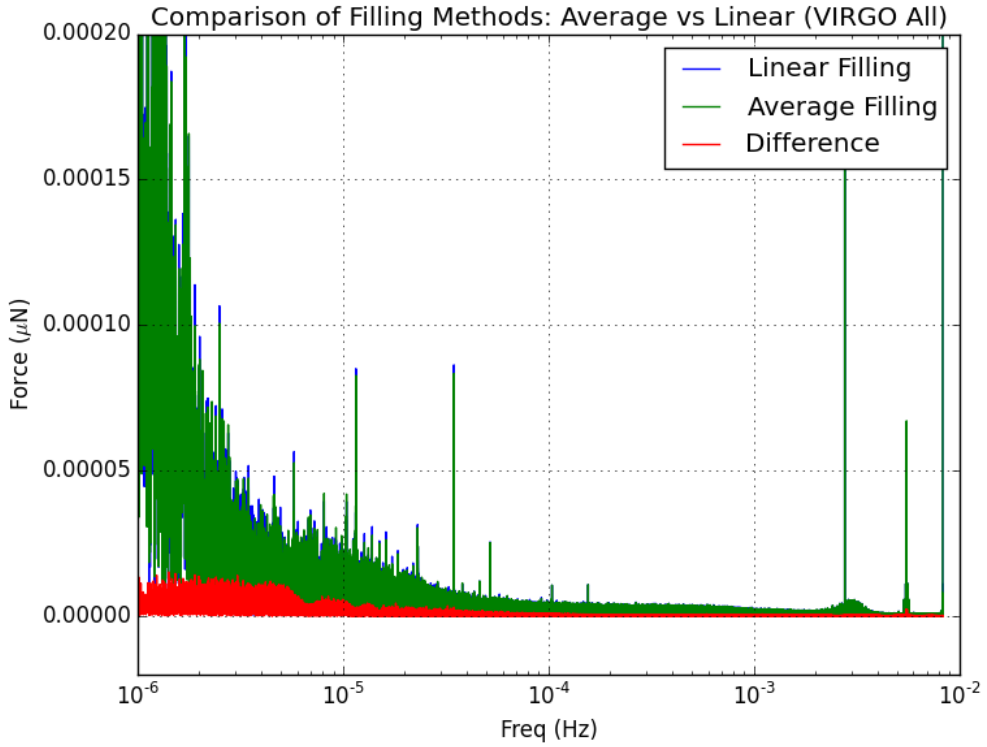

FIG. 10: Visual comparison of both averaging and linear gap filling techniques using the VIRGO dataset.

Now examing the fourier transform of force in figure 12 we can see a bumb around .00300 Hz. Figure 13 provides a closer look. The physical sources of these spikes are from different pressure modes of the sun. With periods 5 minutes, parts of the surface of the sun will move up and down which increases and decreases solar irradiance accordingly. Our results for this section match with scholars who have examined the VIRGO dataset much more closely.[11] We can also clearly see three large spikes within the desired frequency range. This first is right around .00278Hz which is inside the "5-mintue oscillation" frequencies. The other two higher frequencies are .00556 Hz and .00833 Hz. We are sure that these spikes are artificial since they can all be found by

$$f = \frac{1}{n \cdot 60sec}$$

where n is the order of harmonic. This means that all of these spikes are have integer periods (2,3, and 6 times respectively) of the sampling period (60 sec) and we should be skeptical that these are physical frequencies. Assuredly enough, other scholars' results do not contain these spikes so we assumed that aren't physical but some artifact left in the data or introduced by our filling method.[11] This discrepency has not yet been resolved and made more confusing when we produced fourier transforms of known functions and got the correct frequencies. This problem must be settled before publication.

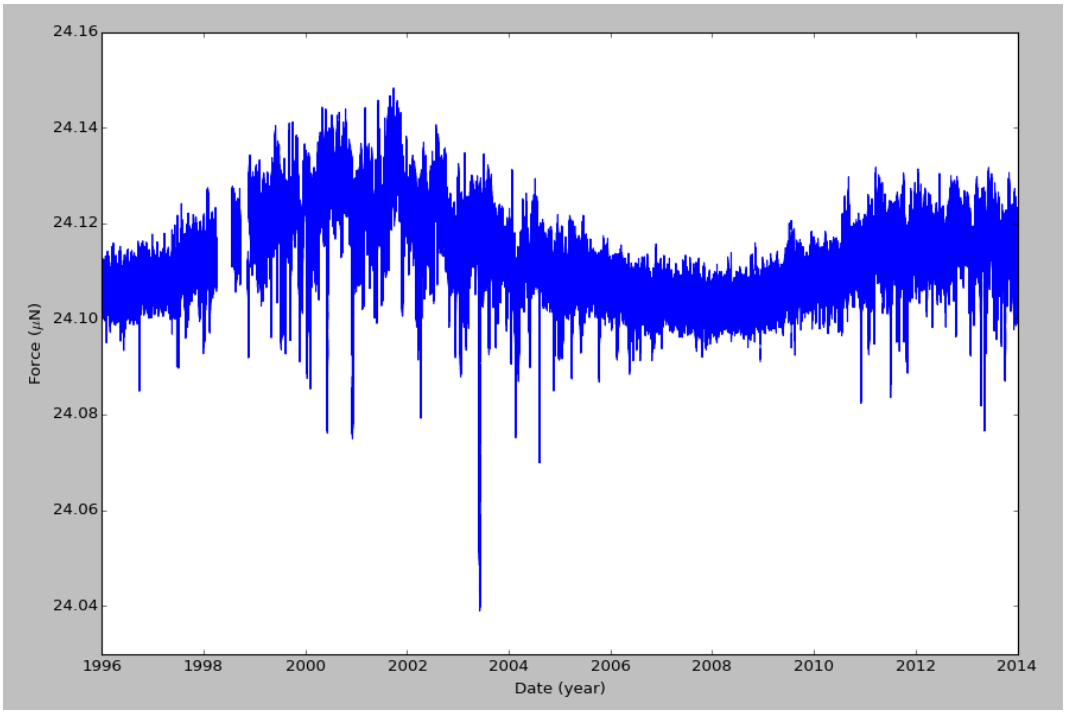

FIG. 11: Total force by solar irradiation on LISA spacecraft calculated from VIRGO data from the period of 1996 to 2014.

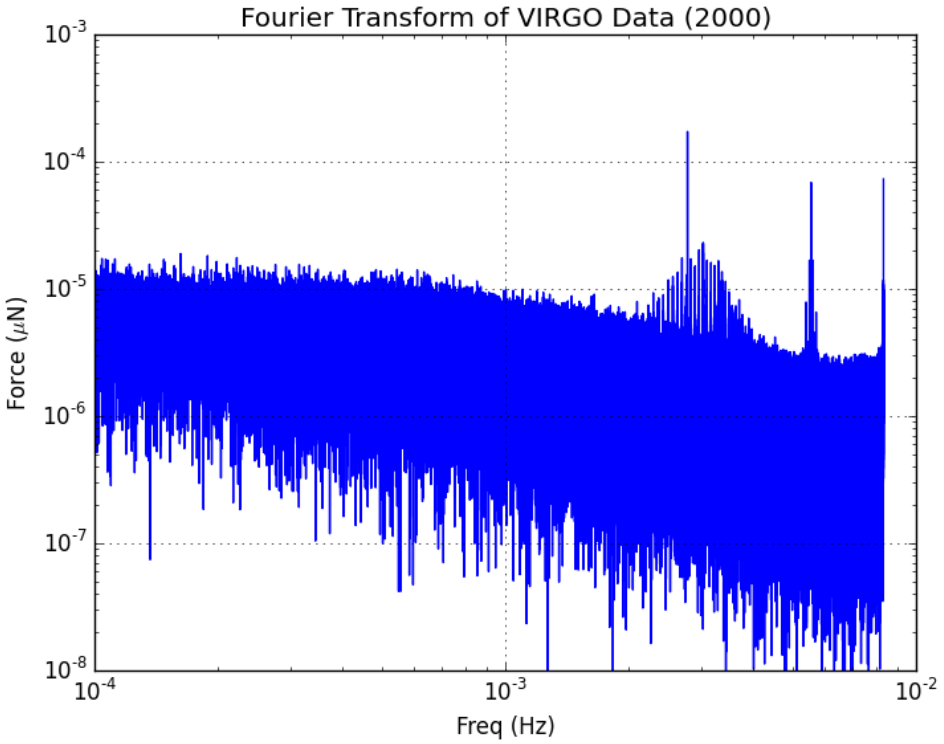

FIG. 12: Fourier transform of the force of year 2000, scaled logarithmically

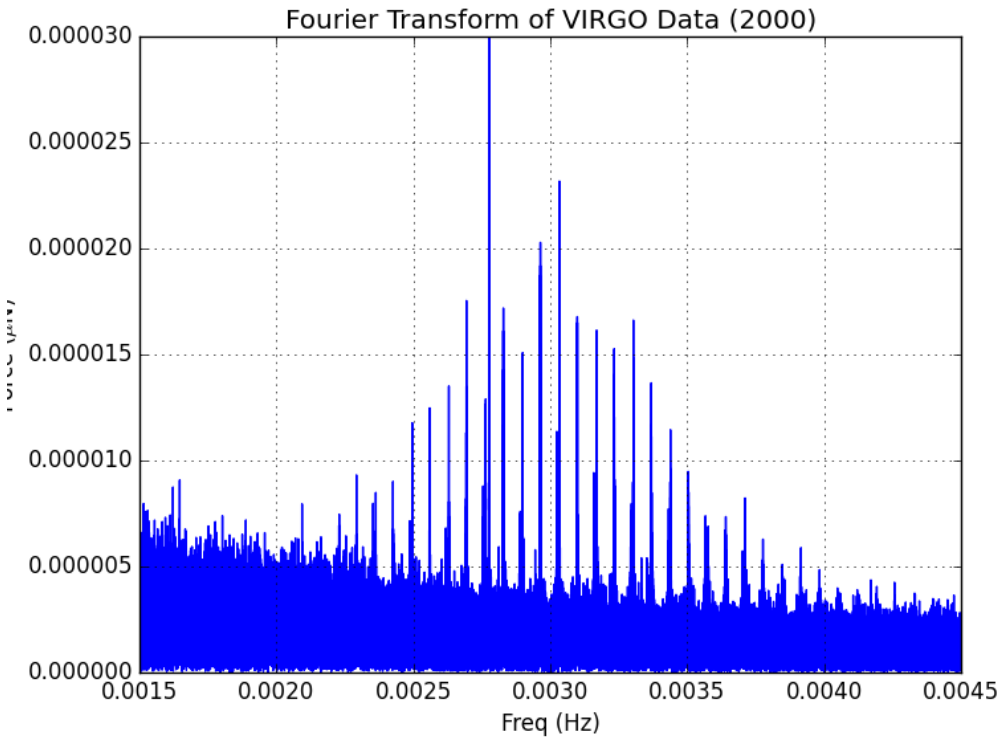

FIG. 13: Fourier transform of the entire VIRGO data set, centered around the "5-minute" solar p-mode oscillations.

VII. REFERENCES

[1] Axel Hammesfahr, et. al. , 2000,"Study of Laser Interferometer Space Antenna," Final Technical Report, http://lisa.nasa.gov/Documentation/FTR.pdf

[2] Purdue, Patricia & Larson, Shane L, 2007, "Spurious Acceleration Noise in Spaceborne Gravitational Wave Interferometers"

[3] Moore, Thomas A., 2013, "A General Relativity Workbook" University Science Books. 352-365.

[4] Abbot, B.P, et. al. , 2016, "Observation of Gravitational Waves from Binary Black Hole Merger," Phys. Rev. Lett. 116.

[5] 2009, "Laser Interferometer Space Antenna (LISA) Mission Concept," NASA-ESA report, http://lisa.nasa.gov/Documentation/LISA-PRJ-RP-0001.pdf

[6] Cutler C., Thorne K. , 2002, "An Overview of Gravitational-Wave Sources," World Scientific, February 26, http://elmer.caltech.edu/ph237/week8/CutlerThorne.pdf

[7] Wright, Jerome L, 1992, "Space Sailing" , Gordon and Breach Science Publishers.

[8] Qioptiq,"Cover Glass Specifications", "Optical Solar Reflector Specifications", Qioptiq solar array manufacturer specifications ,http://www.qioptiq.com/space.html

[9] Osgood, B. , "EE261: The Fourier Transform and its Applications," Electrical Engineering Department: Stanford University. 252-253.

[10] Rubbo, Cornish & Poujade, "Forward Modeling of space-borne gravitational wave detectors"

[11] Stahn, T. , 2010, "Analysis of time series of solar-like oscillations- Applications to the Sun and HD 52265," Georg-August-Universitt zu Gttingen.

Links to Pictures

https://solarsystem.nasa.gov/multimedia/display.cfm?Category=Spacecraft&IM_ID=10685

http://lisa.nasa.gov/Documentation/FTR.pdf

https://upload.wikimedia.org/wikipedia/commons/thumb/a/af/Gravitational-wave_detector_sensitivities_and_astrophysical_gravitational-wave_sources.png/440px-Gravitational-wave_detector_sensitivities_and_astrophysical_gravitational-wave_sources.png

https://www.learner.org/courses/physics/visual/img_full/gravitational_waves.jpg

APPENDIX A: DERIVATION OF FORCE

1. **Force from Irradiation -** Firstly we should note that unlike solar wind, photons are not bent by magnetic fields and simply travel nearly straight from the sun (otherwise we would see the sun in a 'haze,' moving around as wisps or be bent into strange shapes.) Therefore we can assume that the irradiation will be comely solely from the x-direction traveling in the -x-directions. For a perfectly absorbing surface, the force by solar pressure would be

$$\vec{F_I} = -\frac{E_f A}{c}\hat{x} \tag{A1}$$

where E_f is the energy flux or irradiance (W/m^2), A is area ($A = \pi r^2 \cos a$, where a is again the angle between the normal and sun, in this case.) However we must assume that some amount of radiation will instead reflect. Taking r to be our reflectivity constant, we have

$$\begin{aligned}\begin{bmatrix} F_x \\ F_z \end{bmatrix} &= -\begin{bmatrix} \frac{E_f A}{c} + r\frac{E_f A}{c}\cos 2a \\ r\left(\frac{E_f A}{c}\right)\sin 2a \end{bmatrix} \\ &= -\frac{E_f A}{c}\begin{bmatrix} 1 + r\cos 2a \\ r\sin 2a \end{bmatrix}\end{aligned}$$

Note that the rotating terms include $2a$ because light is being reflected, not just rotated. For example, when $a = 45°$ we should the reflected directly upwards so $F_y \propto \sin(2 \cdot 45°) = 1$ and the reflected term in the x-direction goes to zero since $F_{x\ reflective} \propto \cos(2 \cdot 45°) = 0$.

2. **Cutoff Frequencies of Coverglass -** To accomidate for the coverglass rejecting certain frequencies, we must consider the blackbody radiation specturm $u(T, f)$ of the satellite using Planck's Law

$$u(T, f)df = \frac{8\pi k^4 T^4}{c^3 h^3}\frac{\eta^3 d\eta}{e^\eta - 1} \tag{A2}$$

where $u(T, f)df$ is the energy density in the interval $[f, f + df]$ and $\eta = hf/kT$. The rest of the constants are standard: h is Planck's constant ($\approx 6.6 \cdot 10^{-34} Js$), c is the speed of light ($\approx 3.0 \cdot 10^8 m/s$), and k is the Boltzman's constant ($\approx 1.4 \cdot 10^{-23} J/K$). Since we wouldn't want our satellite to get incredibly hot, we will assume that the surface is made of a material that reflects wavelengths smaller than our smallest allowed and larger than our largest allowed. We will consider two cases of these limits: one with (lower wavelength $300nm$ and upper wavelength $1350nm$ based on modern coverglass specifications) and a more extreme case (lower wavelength $300nm$ and upper wavelength $1100nm$ that represent a more ideal coverglass.)

The general fraction of power is then

$$\delta = \int_{\eta_{uv}}^{\eta_{ir}} \frac{\eta^3 d\eta}{e^\eta - 1} \Big/ \int_0^\infty \frac{\eta^3 d\eta}{e^\eta - 1}$$

$$= \int_{\eta_{uv}}^{\eta_{ir}} \frac{\eta^3 d\eta}{e^\eta - 1} \Big/ \frac{\pi^4}{15} \tag{A3}$$

$$\approx .81 \quad \text{(modern coverglass case)}$$
$$\approx .66 \quad \text{(more ideal case)}$$

The functional purpose of δ will be to reduce the absorption constant so our materials act is if they were more reflective (i.e.$\alpha_{new} = \delta\alpha_{old}$).

3. **Force from Irradiation (With Materials) -** Since many sources use a constant of absorbance instead of reflectivity, and α is reserved for this end, we will from now on use a for angle and α for absorbance. Letting $r \approx 1 - \alpha$, assuming minimal diffuse reflection (our material are all glass so this assumption is well founded), our generalized force is now

$$\vec{F_I} = -\frac{E_f A}{c} \begin{bmatrix} 1 + (1-\alpha)\cos 2a \\ (1-\alpha)\sin 2a \end{bmatrix} .$$

However, the solar array is composed of two components: the solar cells and reflective mirrors (OSRs) with different emissivities and absorbances. So we now have

$$F_I = F_{sc} + F_{osr}.$$

Letting α_{sc} and α_{osr} be the respective absorbances of the solar cells and the optical solar reflectors, as well as A_{sc} and A_{osr} be the respective areas of the solar cells and the optical solar reflectors, we have

$$\vec{F_I} = -\frac{E_f}{c} \left(A_{sc} \begin{bmatrix} 1 + (1-\delta\alpha_{sc})\cos 2a \\ (1-\delta\alpha_{sc})\sin 2a \end{bmatrix} + A_{osr} \begin{bmatrix} 1 + (1-\delta\alpha_{osr})\cos 2a \\ (1-\delta\alpha_{osr})\sin 2a \end{bmatrix} \right) \tag{A4}$$

4. **Considerations with Re-radiation** Once the photon is absorbed it will be re-radiated via blackbody radiation in an isotropic fashion with a power determined via the Stefan-Boltzmann law modified by the emissivity ϵ

$$E_f = \epsilon\sigma T^4 .$$

By simply considering the fact that the radiation is isotropic over a hemisphere we can see that the net force must be reduced by a factor of

$$\int_0^{2\pi} \int_0^{\pi} \cos\theta \sin\theta \mathrm{d}\theta \mathrm{d}\phi = \pi.$$

5. **Re-radiation via blackbody -** Before we can calculate the force reradiated from the solar array, we must first find the steady-state temperature of the solar array. When our solar array reaches thermal equilibrium, the amount of power entering the array will equal the power being reradiated so we have

$$0 = \alpha_{sc} A_{front} E_F - A \epsilon_{sc} \sigma T_{sat}^4$$

where ϵ_{sc} and ϵ_{osr} are the respective emissivities of the solar cells and the optical solar reflectors, and A_{front} is the area exposed to radiation. Since $A_{front} = A$ in our case (front area is the only area allowed to reradiate), we solve for T

$$T_{sat} = \left(\frac{\alpha_{sc} E_f}{\epsilon_{sc} \sigma} \right)^{1/4} .$$

Considering the case where we have a cutoff frequency and have two different materials (solar cells and OSR), our starting equation would be

$$0 = \delta \alpha_{sc} A_{sc} E_F + \delta \alpha_{osr} A_{osr} E_F - A_{sc} \epsilon_{sc} \sigma T_{sat}^4 - A_{osr} \epsilon_{osr} \sigma T_{sat}^4$$

Letting $A_r = A_{osr}/(A_{osr} + A_{sc})$ and solving for T, we have now

$$T_{sat} = \left(\delta \frac{\alpha_{sc}(1 - A_r) + \alpha_{osr} A_r}{\epsilon_{sc}(1 - A_r) + \epsilon_{osr} A_r} \frac{E_f}{\sigma} \right)^{1/4} .$$

We note again that since every blackbody will reradiate isotropically, this force will be reduced by a factor of $1/\pi$. Following the Stephan-Boltzman Law we have

$$\begin{bmatrix} F_x \\ F_z \end{bmatrix} = -\frac{1}{\pi} \frac{\epsilon_{sc} \sigma T_{sat}^4}{c} \begin{bmatrix} \cos a \\ \sin a \end{bmatrix}$$

Again if we consider both materials, we have

$$\begin{bmatrix} F_x \\ F_z \end{bmatrix} = -\frac{1}{\pi} \left(\epsilon_{sc}(1 - A_r) + \epsilon_{osr} A_r \right) \frac{\sigma T_{sat}^4}{c} \begin{bmatrix} \cos a \\ \sin a \end{bmatrix} \tag{A5}$$

APPENDIX B: GAP LENGTH GRAPHS

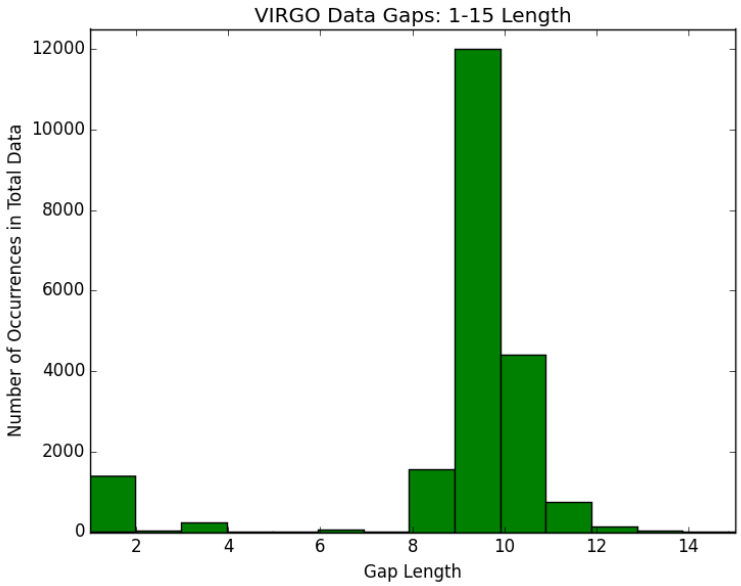

FIG. 14: The number of occurrences per gap length, specifically gaps with lengths of 1-15, in the VIRGO dataset

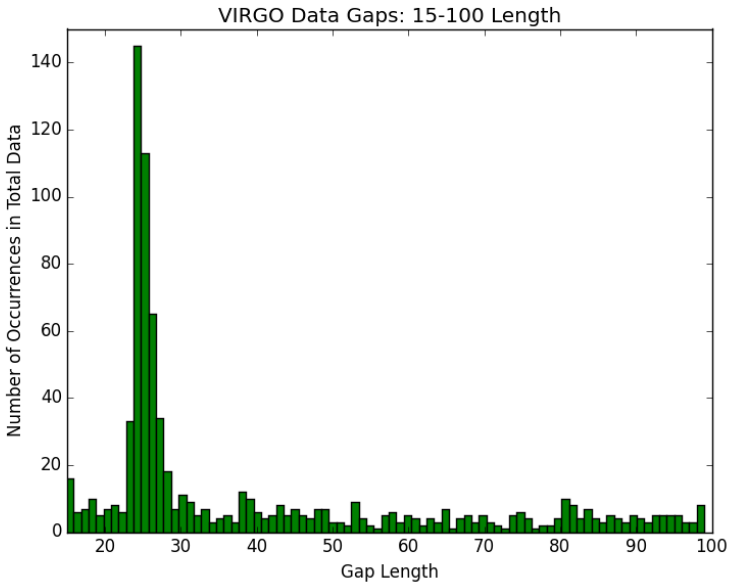

FIG. 15: The number of occurrences per gap length, specifically gaps with lengths of 15-100, in the VIRGO dataset

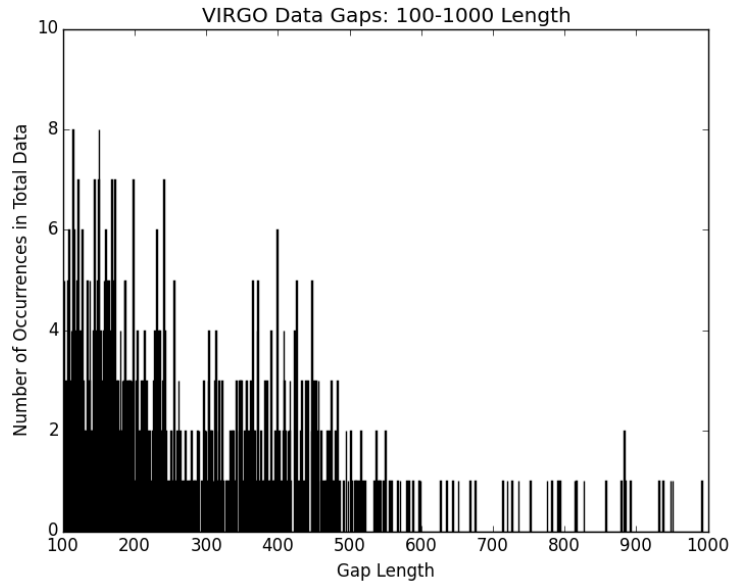

FIG. 16: The number of occurrences per gap length, specifically gaps with lengths of 100-1000, in the VIRGO dataset

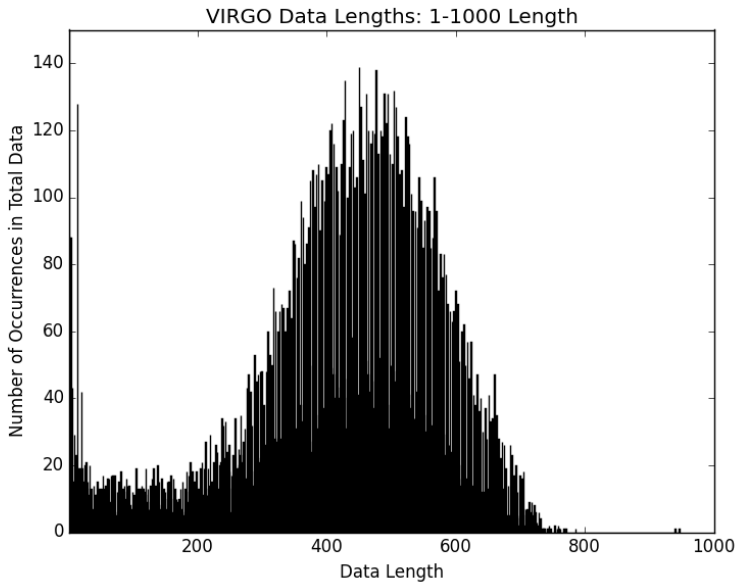

FIG. 17: The number of occurrences per continuous uninterupted data length, specifically data with lengths of 1-1000, in the VIRGO dataset